AD-A139 633 OXIDE BOND ENERGIES FOR THE CALIBRATION OF MATRIX EFFECTS IN SECONDARY IO..(U) CORNELL UNIV ITHACA NY DEPT OF CHEMISTRY A A GALUSKA ET AL. 28 MAR 84 TR-13 1/1

UNCLASSIFIED N00014-80-C-0538 F/G 20/12 NL

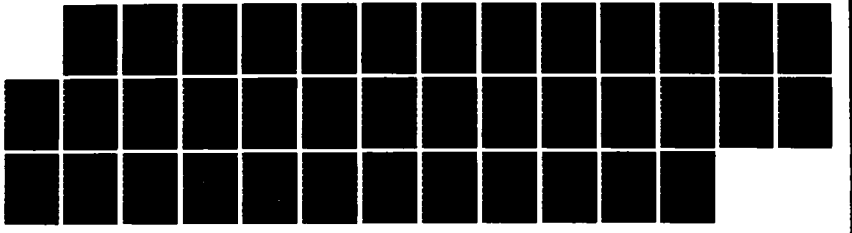

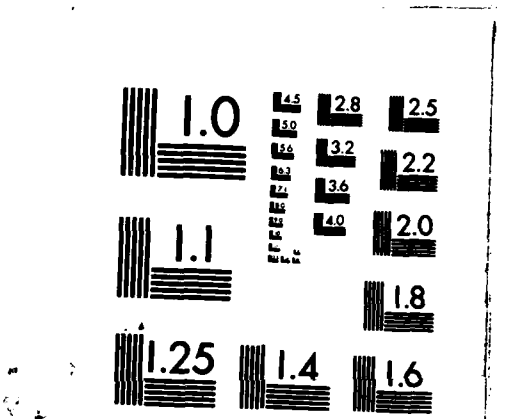

SECURITY CLASSIFICATION OF THIS PAGE (When Data Entered)

REPORT DOCUMENTATION PAGE

READ INSTRUCTIONS BEFORE COMPLETING FORM

1. REPORT NUMBER	2. GOVT ACCESSION NO.	3. RECIPIENT'S CATALOG NUMBER
Technical Report #13	AD-A139633	

4. TITLE (and Subtitle)

OXIDE BOND ENERGIES FOR THE CALIBRATION OF MATRIX EFFECTS IN SECONDARY ION MASS SPECTROMETRY

5. TYPE OF REPORT & PERIOD COVERED

Interim Technical Report

6. PERFORMING ORG. REPORT NUMBER

7. AUTHOR(s)

A. A. GALUSKA AND G. H. MORRISON

8. CONTRACT OR GRANT NUMBER(s)

N00014-80-0538

9. PERFORMING ORGANIZATION NAME AND ADDRESS

DEPT. OF CHEMISTRY
CORNELL UNIVERSITY, ITHACA, NEW YORK 14853

10. PROGRAM ELEMENT, PROJECT, TASK AREA & WORK UNIT NUMBERS

NR051-736

11. CONTROLLING OFFICE NAME AND ADDRESS

ONR (472)
800 N. Quincy St., Arlington, VA 22217

12. REPORT DATE

March 28, 1984

13. NUMBER OF PAGES

36

14. MONITORING AGENCY NAME & ADDRESS(if different from Controlling Office)

15. SECURITY CLASS. (of this report)

unclassified

15a. DECLASSIFICATION/DOWNGRADING SCHEDULE

16. DISTRIBUTION STATEMENT (of this Report)

APPROVED FOR PUBLIC RELEASE: DISTRIBUTION UNLIMITED

17. DISTRIBUTION STATEMENT (of the abstract entered in Block 20, if different from Report)

18. SUPPLEMENTARY NOTES

PREPARED FOR PUBLICATION IN INTERNATIONAL JOURNAL OF MASS SPECTROMETRY AND ION PROCESSES

19. KEY WORDS (Continue on reverse side if necessary and identify by block number)

3-5 compound semiconductors
Secondary Ion Mass Spectrometry
Matrix Calibration
Ion Yields
Oxygen Affinity
Quantitative Analysis
Qualitative Analysis

20. ABSTRACT (Continue on reverse side if necessary and identify by block number)

Analyses of trace and major elements in group III-V compound matrices by secondary ion mass spectrometry (SIMS) have shown that practical ion yields are linearly related to the matrix composition. The affinity of the matrix to oxygen appears to be the critical factor in this relationship. A direct relationship between the slopes of these calibration lines, determined for elements in the same column of the periodic table, and the first ionization potential of the respective elements has also been shown.

DD FORM 1 JAN 73 1473

SECURITY CLASSIFICATION OF THIS PAGE (When Data Entered)

OXIDE BOND ENERGIES FOR THE CALIBRATION OF MATRIX EFFECTS IN SECONDARY ION MASS SPECTROMETRY

A. A. Galuska and G. H. Morrison*

Department of Chemistry
Cornell University
Ithaca, New York 14853

ABSTRACT

Analyses of trace and major elements in group III-V compound matrices by secondary ion mass spectrometry (SIMS) have shown that practical ion yields are linearly related to the matrix composition. The affinity of the matrix to oxygen appears to be the critical factor in this relationship. A direct relationship between the slopes of these calibration lines, determined for elements in the same column of the periodic table, and the first ionization potential of the respective elements has also been shown.

Secondary ion mass spectrometry (SIMS) is a powerful technique for the analysis of thin solid films. It has ppm sensitivity for most elements, excellent depth resolution (<100 Å), and good lateral resolution (about 1.0 μm). Using standards prepared by ion implantation, quantitative analyses accurate to about 15% can be obtained for trace elements (<0.1 atomic percent) in homogeneous matrices [1-3]. Due to matrix effects, however, the standard must match the sample matrix. This not always convenient or possible. In addition, the quantification of SIMS depth profiles in multilayer-multimatrix samples remains a problem due to the changing practical ion yields and sputtering yields which are encountered.

For $Al_xGa_{1-x}As$ and related matrices, it has recently been shown that relative ion yields ($R\tau$) and relative sputtering yields (RS) vary linearly with sample composition [4]. The relative values were obtained by normalizing practical ion yields (τ) and sputtering yields (S) from a sample matrix to those from a standard matrix when both measurements were performed under nearly identical analysis conditions. By this procedure, precise calibration lines have been obtained, and subsequently been applied to a variety of $Al_xGa_{1-x}As$ superlattices using the depth profile correction program SLIC (superlattice and interface calibration) [5].

The general application of such a calibration method to a greater variety of matrices requires an understanding of the fundamental processes involved. There are currently two principal hypotheses for

the variation of τ's with matrix. It has been suggested that matrix effects are primarily a function of sputtering yields [6, 7]. Lower S's enhance the build-up of reactive primary ions (O_2^+ or Cs^+) in the surface resulting in increased τ's. This hypothesis is expressed in eq. 1

$$R\tau_g \propto (1/RS)^y \qquad (1)$$

where y is a constant determined experimentally for the analyte g. Others have asserted that under certain conditions τ's are a linear function of matrix composition [8, 9]. This compositional approach is expressed in eq. 2

$$R\tau_g \propto \sum_{i=1}^{n} P_{i,g} C_i \qquad (2)$$

where n is the number of elements in the matrix, C_i is the atomic fraction of element i in the matrix, and $P_{i,g}$ is a dimensionless parameter representing the influence of element i on the ion yield of element g. In addition, a strong correlation between the mean free energies of matrix-oxygen bonds and the observed trends in ionization probabilities has been reported for certain binary metal alloys [10, 11].

In the present study, these principal explanations for the variation of τ's with matrix were investigated using Rτ's from trace and major elements in various group III-V compound matrices. A strong relationship between Rτ's and RS's was not observed. Alternatively, a very strong linear relationship was found between the Rτ's and the average bond energies of the sample matrices to oxygen. Similar linearity was found during Ar^+ bombardment with a high ambient oxygen pressure in the sample chamber. For elements in the same column of the periodic table, a direct correlation was observed between the slopes of these lines and the ionization potentials of the corresponding analytes. Using these trends, it is possible to predict when matrix effects will be a problem. Then, using the appropriate calibration lines it is possible to correct for these matrix effects.

EXPERIMENTAL

Sample Preparation. The $Al_xGa_{1-x}As$, $Ga_{.47}In_{.53}As$, GaSb, and InSb matrices were grown by molecular beam epitaxy (MBE) on semi-insulating GaAs, InP, GaAs, and InSb substrates, respectively. Semi-insulating InP and GaP substrates were also used as sample matrices. The matrix compositions were determined from MBE growth parameters and verified to an accuracy of better than 10% [12] using Rutherford backscattering (RBS) and photoluminescence spectroscopies. Trace elements were introduced using ion implantation. Generally, two different elements

were implanted into each sample. Prior to implantation samples were cleaned with trichloroethylene. The implantation parameters are listed in Table 1.

Instrumentation. SIMS analysis was carried out on a CAMECA (103, Boulevard Saint-Denis, 92403 Courbevoie Cedex, France) IMS-3F ion microanalyzer using an electron multiplier in the pulse counting mode for signal detection [13]. The instrument comes interfaced to a HEWLETT PACKARD (3404 East Harmony Road, Fort Collins, Colorado 80525) 9845T microcomputer for control and data acquisition. The experimental parameters are listed in Table 2. To avoid saturating the electron multiplier, the sampling area was reduced to 5.0×10^{-7} cm^2 when $^{27}Al^+$, $^{69}Ga^+$, $^{7}Li^+$, and $^{24}Mg^+$ were analyzed. A multiple sample holder was used to simultaneously mount several samples. Depth measurements on the sputtered craters were performed using a mechanical stylus.

Software. Programs for instrumental control, data analysis, and matrix correction were written in BASIC for the HEWLETT PACKARD 9845T.

Procedure. Following ion implantation, 4 to 7 samples were simultaneously mounted and depth profiled using a multiple sample holder. Each group of samples included GaAs as a standard matrix for ion yield and sputtering yield normalization. The samples were inserted simultaneously to insure nearly identical analysis conditions. After allowing the pressure in the sample chamber to

reach a steady state condition, the O_2^+ primary ion beam was focused, and the proper mass settings were determined. Without manipulating any instrumental parameters, the samples were analyzed consecutively until at least 3 profiles of each sample had been made. τ's, Rτ's, S's, and RS's were determined using standard procedures [4]. The τ's and Rτ's for ^{11}B, ^{31}P, and ^{75}As were also determined using an Ar^+ primary ion beam while the sample chamber was flooded with oxygen to a pressure of 5×10^{-5} torr.

RESULTS AND DISCUSSION

Since Rτ's are linearly related to both RS's and sample composition for $Al_xGa_{1-x}As$ matrices [4], the alteration of τ's with matrix can be explained by either of the two hypotheses of matrix effects. The validity and applicability of these two can only be evaluated by extending the calibration to other group III-V compound matrices. The sputtering yield hypothesis was evaluated directly. The compositional approach was evaluated using the observation of Yu and Reuter [10, 11] that the affinity of a matrix for oxygen (ΔG_f metal oxide) determines the influence of a particular matrix composition on τ's. Consequently, the parameter $P_{i,g}$ was treated as a measure of the affinity of element i for oxygen.

The exact forms of the metal-oxygen complexes which are created

during the sputtering process are difficult to determine. Consequently, the free energies of metal oxide formation were not used as an indicator of oxygen affinity. Instead, this affinity was roughly approximated using the bond energies of the diatomic metal oxides. Preliminary analysis indicated that a linear relationship existed between τ's and the oxygen affinity of the matrices, but that this linearity could be improved for all analytes by using slightly modified bond energy values as an indicator of oxygen affinity. These modified bond energy values are used throughout the paper. The literature values [14] and the modified values of these bond energies are given in Table 3.

The two approaches to the problem of matrix effects are compared in Figures 1-4 for ^{28}Si, ^{9}Be, ^{31}P, and ^{24}Mg in various group III-V semiconductors. According to the compositional theory, plots of $R\tau$ versus the average matrix-oxygen bond energy should yield straight lines. Similarly, according to the sputtering yield hypothesis, plots of $\log(R\tau)$ versus $\log(1/RS)$ should also yield straight lines. As apparent in these figures, the compositional theory satisfies this criterion much better than the sputtering yield approach. In fact, the linearity that is apparent in the plots of $\log(R\tau)$ versus $\log(1/RS)$ can be attributed almost entirely to the linearity expected for the $Al_xGa_{1-x}As$ data points. The linear correlations and relative standard deviations of the slopes of these two types of plots are presented in Table 4. The linear correlations of the compositional approach are quite superior to those of the sputtering yield approach.

In addition, the relative standard deviations of the slopes obtained by the sputtering yield method were many times larger than those obtained by the compositional method.

Certainly, these experimental data favor the compositional approach. If, however, matrix effects in these samples are determined by the affinity of the samples for oxygen, one would also expect a linear relationship between $R\tau$'s and the average matrix-oxygen bond energies when an Ar^+ primary ion beam is used in conjunction with oxygen flooding. Such an investigation was carried out on ^{11}B, ^{31}P, and ^{75}As under conditions short of oxygen saturation. As apparent in Table 5, the linear relationship between $R\tau$'s and these bond energies is maintained as expected despite the different analysis conditions. In fact, as shown in Table 6, the slopes of the ^{11}B, ^{31}P, and ^{75}As calibration lines under both types of bombardment are very similar. The differences that are apparent can most likely be attributed to the under saturation of the sample matrices with oxygen. With the addition of these corroborating data, it appears that matrix effects in group III-V semiconductors are a linear function of the sample composition and in particular the affinity of a particular matrix to oxygen. Oxygen flooding and the O_2^+ bombardment process control the availability of oxygen, but the oxygen affinity of the matrix determines the extent of oxidation. For $Al_xGa_{1-x}As$ [4, 5, 15] and other group III-V semiconductors, the oxygen affinity is the most critical factor influencing matrix effects.

In addition to determining a general mechanism for matrix effects, it is also important to understand how matrix effects influence the τ's of one particular element versus another. One can gain an insight into this phenomenon by comparing the slopes of the calibration lines to the first ionization potentials of the respective analytes. Such a comparison is presented in Table 6. At first glance, there is no apparent relationship between the slopes and the first ionization potentials. However, upon examining just those elements which fall in the same column of the periodic table [(B, Al, Ga),(P, As, Sb), and (Be, Mg)], a general relationship is observed. Those elements with higher first ionization potentials yield calibration lines of steeper slope than those with lower first ionization potentials. This indicates that elements which have a small ionization probability are influenced by matrix effects (the amount of bound oxygen) to a greater extent than those which have a large ionization probability. As one might expect, this relationship is very similar to that commonly observed for elemental τ's in a single matrix enhance by oxygen bombardment or flooding: elements that have a small ionization probability are enhanced to a greater extent by the presence of oxygen than those that have a large ionization probability. Thus, the relationship between the slopes of these calibration lines and the first ionization potentials is intuitive.

Application. The excellent linearity of the $R\tau$ versus matrix-oxygen bond energy calibration lines and their relationship to

elemental ionization potentials can be used to improve the quality of both qualitative and quantitative SIMS analysis. Using the relationships expressed in these matrix calibration lines, one can anticipate when matrix effects will be a problem, and how they may distort depth profiles of layered multimatrix samples. For example, a largely distorted gaussian depth distribution would be expected for a ^{11}B implant through a GaAs layer into an $Al_xGa_{1-x}As$ layer because ^{11}B is very sensitive to the presence of oxygen, i.e. matrix effects, and $Al_{.3}Ga_{.7}As$ has a much greater oxygen affinity than GaAs. Alternatively, a smaller distortion would be expected for an ^{24}Mg implant and an even smaller distortion for an ^{7}Li implant into such a structure. The sensitivity of these elements to matrix effects decreases going from ^{11}B to ^{24}Mg to ^{7}Li. The SIMS analyses of these implants are shown in Figure 5.

When a quantitative SIMS analysis in either a single matrix or a layered multimatrix sample is desired, these calibration lines can be quite valuable. Since these types of calibration lines are reproducible [4], dopant distributions in a homogeneous group III-V compound matrix can be quantified using the calibration lines and a single standard prepared from any of the group III-V compound matrices. There is no need to make a separate standard for each matrix. These calibration lines can also make the quantitative SIMS analysis of layered multimatrix samples possible. For very complex layered multimatrix samples, these matrix calibration lines may be inserted into a variation of the program SLIC [5] for matrix

correction. For simpler structures with just a few well defined interfaces, one can treat the interfaces as linear concentration gradients from one matrix to another. Both approaches are presented in Figure 6. A ^{9}Be concentration plateau approximately 0.1 μm wide and $1 - 2 \times 10^{18}$ atom/cm^3 high was grown by MBE while the matrix was linearly changed from GaAs to $Al_{.3}Ga_{.7}As$. In the uncorrected profile, the ^{9}Be distribution (dashed line) resembles a sharp spike rather than a plateau. In addition, the thickness and peak concentration of the plateau can not be determined. The shape of the plateau differs slightly between the two versions of the corrected profile. However, both types of corrections allow a dramatic improvement over the uncorrected profile in the determination of plateau thickness and peak concentration.

In summary, the influence of matrix effects on ion yields in group III-V compound matrices can be precisely calibrated. A compositional approach to matrix calibration based on the oxygen affinity of the sample fits the experimental data quite well while the sputtering yield approach did not. The influence of matrix effects on elements in each column of the periodic table was shown to be directly related to the first ionization potential of the analytes. Finally, the relationships observed can be used to improve the quality of both qualitative and quantitative SIMS analyses.

ACKNOWLEDGMENT

The authors gratefully acknowledge the assistance of B. Shaft for the growth of the MBE matrices, and S. Asher and J.T. Brenna for helpful discussions. The ion implantation was performed at the National Research and Resource Facility for Submicron Structures at Cornell.

CREDIT

This work was supported by the National Science Foundation and the Office of Naval Research.

LITERATURE CITED

1 W.H. Gries, Int. J. Mass Spectrum. Ion Phys., 30 (1979) 97.

2 D.P. Leta and G.H. Morrison, Anal. Chem., 52 (1980) 514.

3 D.P. Leta and G.H. Morrison, Anal. Chem., 52 (1980) 277.

4 A.A. Galuska and G.H. Morrison, Anal. Chem., 55 (1983) 2051.

5 A.A. Galuska and G.H. Morrison, Anal. Chem., 56 (1984) 74.

6 V.R. Deline, W. Katz, C.A. Evans and P. Williams, Appl. Phys. Lett., 33 (1978) 832.

7 V.R. Deline, C.A. Evans and P. Williams, Appl. Phys. Lett., 33 (1978) 578.

8 G. Slodzian, in, Proc. 3rd Int. Conf. Secondary Ion Mass Spectrometry (SIMS III), Springer-Verlag, New York, 1981, p. 115.

9 I. Steele, R. Herrig and I. Hutcheon, in, Proc. 15th Ann. Conf. Microbeam Analysis Society, San Francisco, CA, 1980, p. 151.

10 M.L. Yu and W. Reuter, J. Appl. Phys., 52 (1981) 1478.

11 M.L. Yu and W. Reuter, J. Appl. Phys., 52 (1981) 1489.

12 J.W. Mayer, J.F. Ziegler, L.L. Chang, R. Tsu and L. Esaki, J. Appl. Phys., 44 (1973) 2322.

13 J.M. Ruberol, M. Lepareur, B. Autier, J.M. Gourgout, in, VIIIth Int. Cong. X-ray Optics and Microanalysis and 12th Ann. Conf. Microbeam Analysis Society, Boston, MA, 1977, p. 133A.

14 L. Brewer and E. Brackett, Chem. Rev., 61 (1961) 425.

15 C. Meyer, M. Maier and D. Bimberg, J. Appl. Phys., 54 (1983) 2672.

Table 1

Ion Implantation Parameters

Implant Element	Fluence ($atom/cm^2$)	Energy (keV)	Source
^{9}Be	1×10^{14}	250	Be solid
^{11}B	1×10^{14}	250	BF_3 gas
^{28}Si	1×10^{15}	250	SiF_4 gas
^{31}P	1×10^{15}	300	PF_3 gas
^{121}Sb	2×10^{14}	250	Sb solid
^{24}Mg	1×10^{15}	300	Mg solid
^{7}Li	1×10^{14}	150	Li solid

Table 2

SIMS Experimental Parameters

Primary Ion: O_2^+, Ar^+

Primary Ion Energy: 5.5 keV

Primary Ion Current Density: ~2.5 X 10^{-2} A/cm^2

Raster: 300 X 300 μm or 400 X 400 μm

Sampling Area: 2.83 X 10^{-5} cm^2

Energy Window: 130 eV

Residual Sample Chamber Pressure: 3 X 10^{-8} torr

Table 3

Matrix Element-Oxygen Bond Energies

Matrix Element	Literature Values (kcal/mole)	Modified Values (kcal/mole)
Al	116 ± 5	116.0
Ga	68 ± 15	68.0
In	≤77	67.0
P	120 ± 4	115.0
As	115 ± 3	115.0
Sb	89 ± 20	114.6

Table 4

Linearity of the Sputtering Yield and
Compositional Approaches to Matrix Calibration
for Group III-V Compound Matrices
Under O_2^+ Bombardment

Log (Rτ) Versus Log (1/RS)

Analyte	Linear Correlation r^2	RSD Slope %
^{28}Si	0.633	64.9
^{9}Be	0.713	54.1
^{31}P	0.731	30.8
^{24}Mg	0.748	21.1

Rτ Versus Matrix-Oxygen Bond Energy

Analyte	Linear Correlation r^2	RSD Slope %
^{28}Si	0.999	0.28
^{9}Be	0.998	0.42
^{31}P	0.991	0.24
^{24}Mg	0.993	0.60

Table 5

Linearity of Rt Versus Matrix-Oxygen Bond Energy
For Group III and V Compound Matrices
Under Ar+ Bombardment With Oxygen Flooding

Analyte	Linear Correlation r^2	RSD Slope %
^{11}B	0.953	0.27
^{31}P	0.928	0.432
^{75}As	0.927	0.505

Table 6

Dependence of Rt Versus Bond Energy Line Slopes
On First Ionization Potential

Under O_2^+ Bombardment

Analyte	Slope	Intercept	1st Ionization Potential (eV)
^{11}B	1.90	-173	8.30
^{27}Al	0.19	- 17	5.98
^{69}Ga	0.25	- 22	6.00
^{31}P	0.93	- 84	11.02
^{75}As	0.30	- 26	9.81
^{121}Sb	0.30	- 26	8.64
^{9}Be	1.86	-169	9.32
^{24}Mg	0.52	- 47	7.64
^{28}Si	1.88	-170	8.15
^{7}Li	0.10	- 9	5.39

Under Ar^+ Bombardment with Oxygen Flooding

^{11}B	1.88	-170	8.30
^{31}P	0.65	- 58	11.02
^{75}As	0.24	- 21	9.81

FIGURE CAPTIONS

Figure 1. Influence of matrix effects on the τ's of ^{28}Si. (a) sputtering yield approach; (b) compositional approach {$Al_xGa_{1-x}As$ - ●, InP - ▲, InSb - ◆, GaP - ■, GaSb - ×}.

Figure 2. Influence of matrix effects on the τ's of ^{9}Be. (a) sputtering yield approach; (b) compositional approach {$Al_xGa_{1-x}As$ - ●, InP - ▲, InSb - ◆, GaP - ■, GaSb - ×}.

Figure 3. Influence of matrix effects on the τ's of ^{31}P. (a) sputtering yield approach; (b) compositional approach {$Al_xGa_{1-x}As$ - ●, InP - ▲, InSb - ◆, GaP - ■, $Ga_{.47}In_{.53}As$ - +}.

Figure 4. Influence of matrix effects on the τ's of ^{24}Mg. (a) sputtering yield approach; (b) compositional approach {$Al_xGa_{1-x}As$ - ●, Inp - ▲, InSb - ◆, GaP - ■}.

Figure 5. SIMS analysis of ^{11}B, ^{24}Mg, and ^{7}Li implants through an GaAs/$Al_xGa_{1-x}As$ structure. (a) depth profiles of $^{11}B^+$ (----) and $^{75}As^+$ (....) {interface at 31 time units}; (b) depth profiles of $^{24}Mg^+$ (----), $^{7}Li^+$ (- - -), and $^{75}As^+$ (....) {interface at 20 time units}.

Figure 6. SIMS analysis of a Be plateau at an GaAs/$Al_{.3}Ga(.7)As$ interface. (a) the hypothetical Be (- - -) {1 - 2 X 10^{18} atom/cm^3 peak conc.} and Al (——) {6.7 X 10^{21} atom/cm^3 peak conc.} structure; (b) uncorrected profile of $^{9}Be^+$ (- - -) and ^{75}As (——); (c) corrected profiles of Be (- - -) {2 X 10^{18} atom/cm^3 full scale} and Al (——) {1 X 10^{22} atom/cm^3 full scale} obtained assuming a linear concentration gradient at the interface; (d) corrected profiles of Be (- - -) {2 X 10^{18} atom/cm^3 full scale} and Al (——) {1 X 10^{22} atom/cm^3 full scale} obtained using the program SLIC.

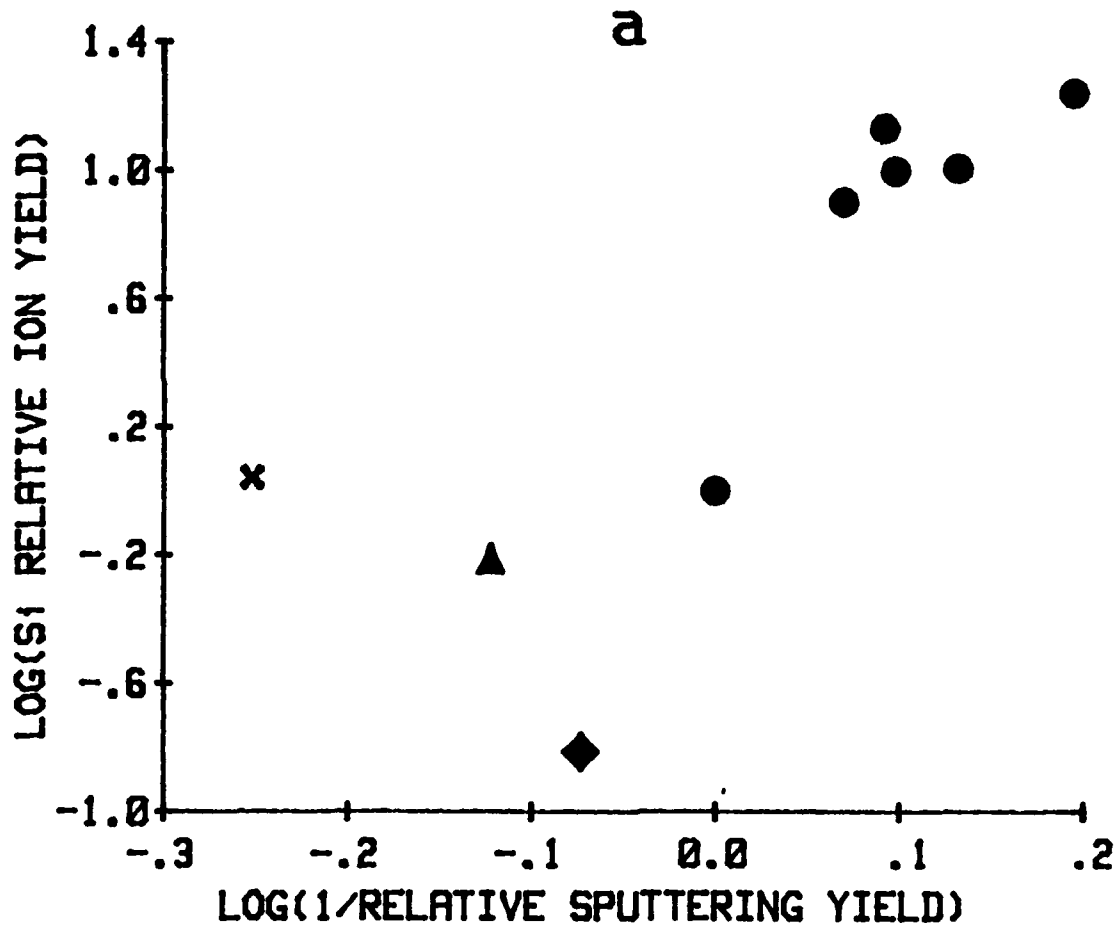
a
1.4
1.0
.6
.2
-.2
-.6
-1.0
-.3
-.2
-.1
0.0
.1
.2
LOG(SI RELATIVE ION YIELD)
LOG(1/RELATIVE SPUTTERING YIELD)

Fig 1a

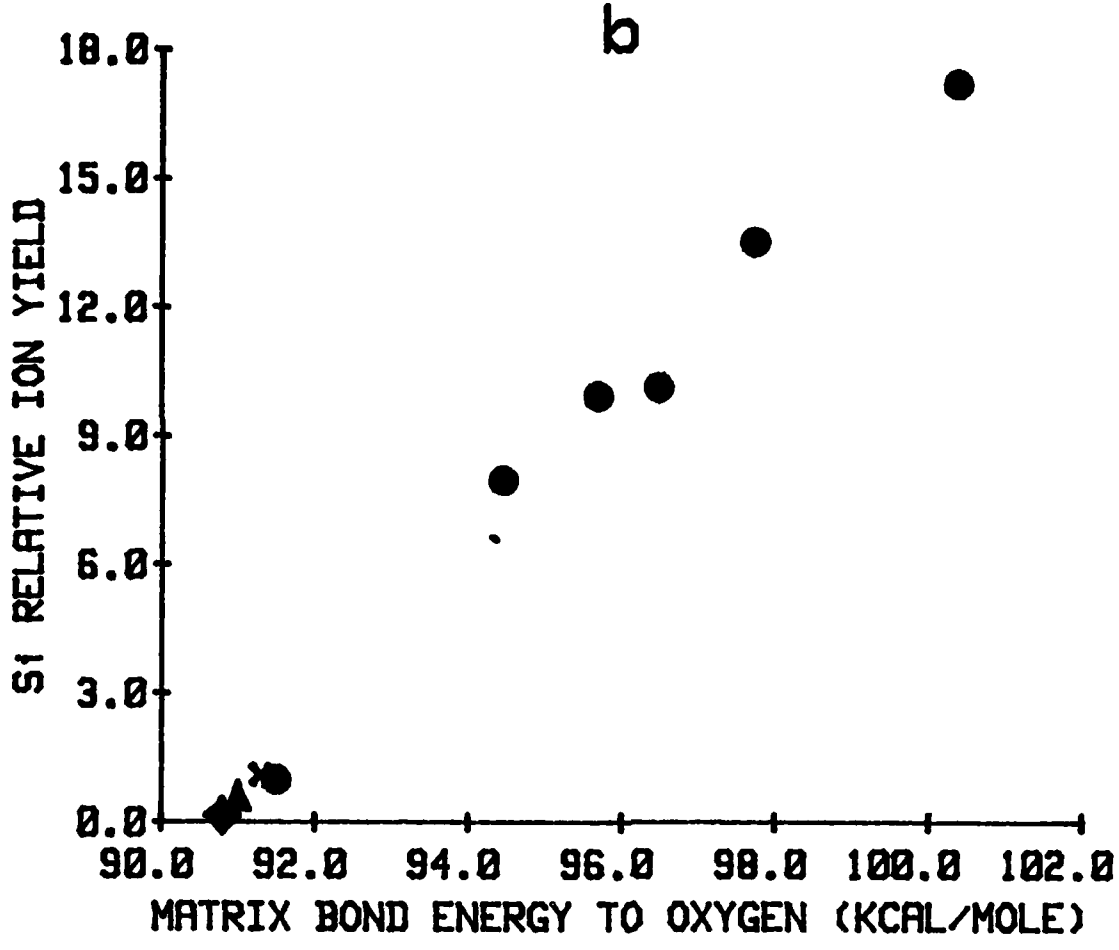
b
18.0
15.0
12.0
9.0
6.0
3.0
0.0
Si RELATIVE ION YIELD
90.0
92.0
94.0
96.0
98.0
100.0
102.0
MATRIX BOND ENERGY TO OXYGEN (KCAL/MOLE)

Fig 1b

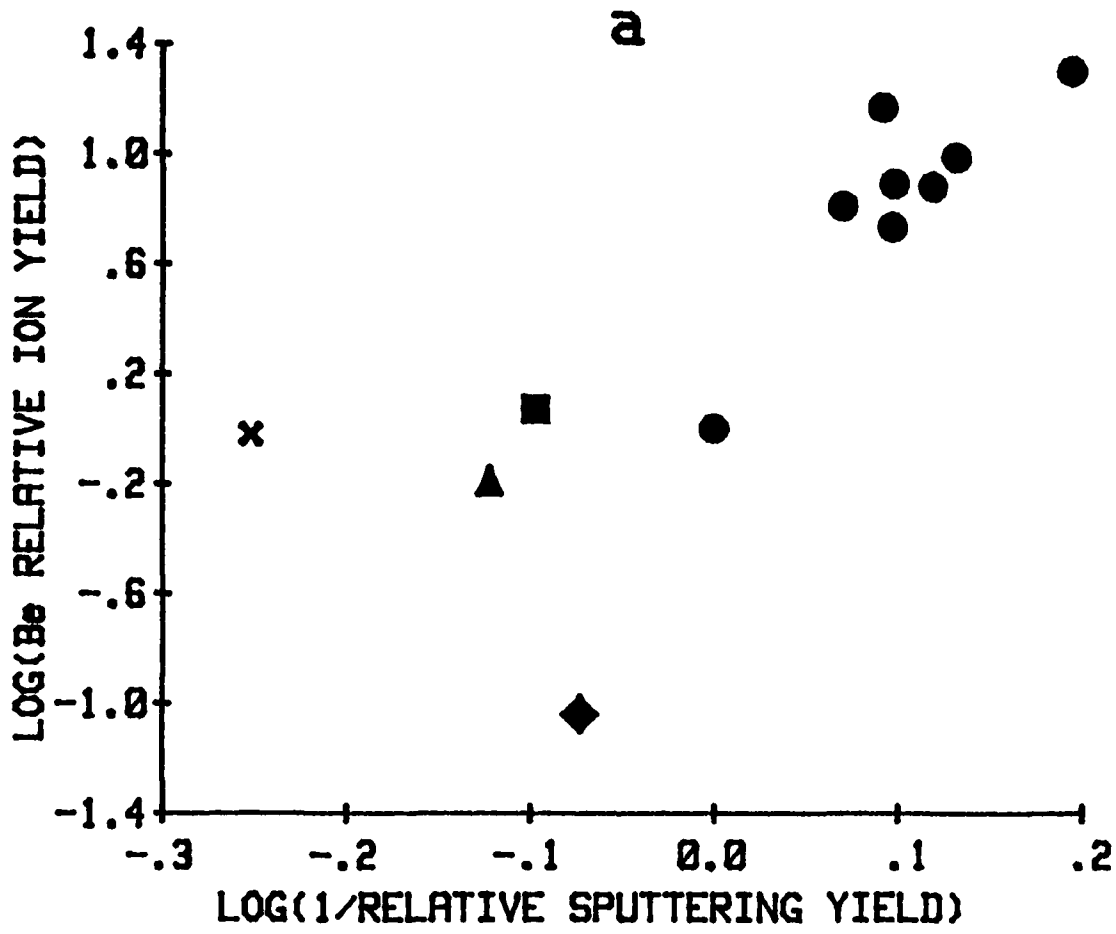
a
1.4
1.0
.6
.2
-.2
-.6
-1.0
-1.4
LOG(Be RELATIVE ION YIELD)
-.3
-.2
-.1
0.0
.1
.2
LOG(1/RELATIVE SPUTTERING YIELD)

Fig 29

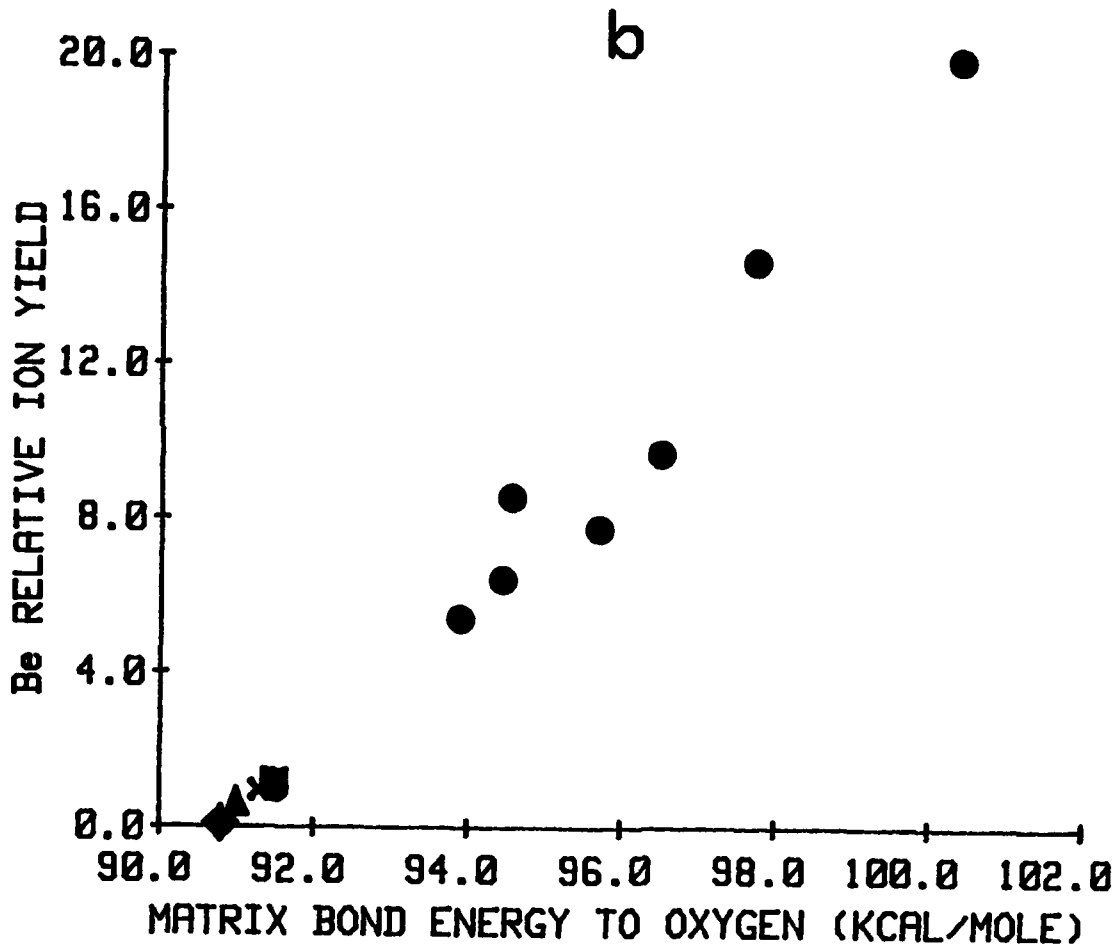
b
20.0
16.0
12.0
8.0
4.0
0.0
Be RELATIVE ION YIELD
90.0
92.0
94.0
96.0
98.0
100.0
102.0
MATRIX BOND ENERGY TO OXYGEN (KCAL/MOLE)

Fig 26

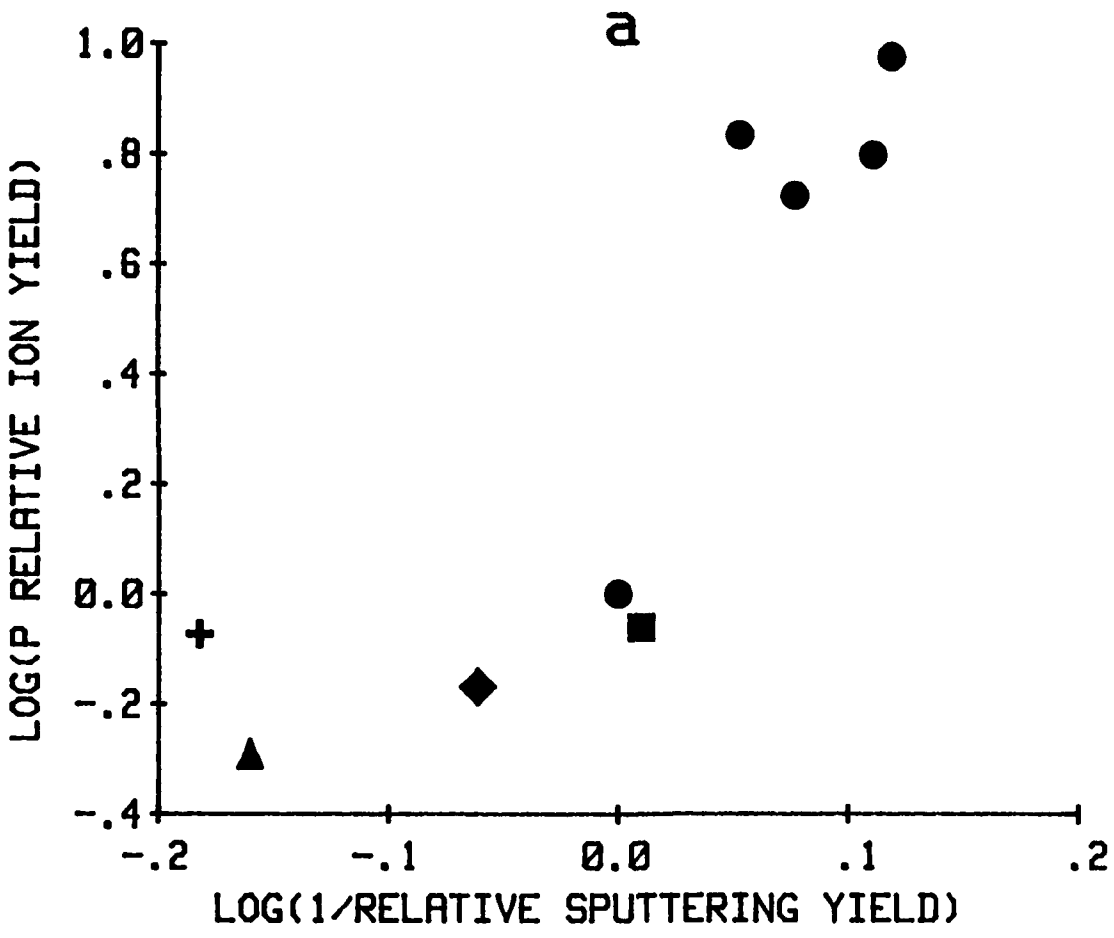
a
1.0
.8
.6
.4
.2
0.0
-.2
-.4
LOG(P RELATIVE ION YIELD)
-.2
-.1
0.0
.1
.2
LOG(1/RELATIVE SPUTTERING YIELD)

Fig 3a

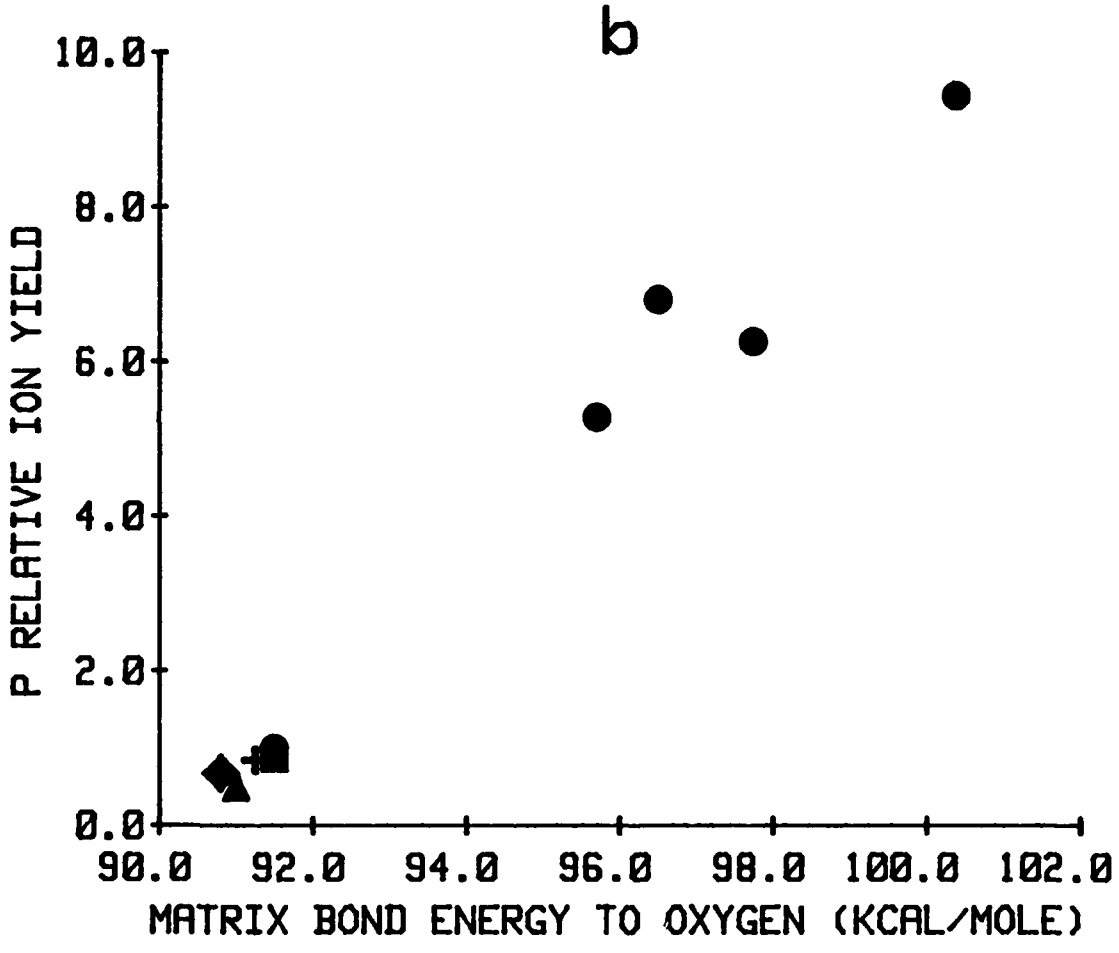
b
10.0
8.0
6.0
4.0
2.0
0.0
P RELATIVE ION YIELD
90.0
92.0
94.0
96.0
98.0
100.0
102.0
MATRIX BOND ENERGY TO OXYGEN (KCAL/MOLE)

Fig 3b

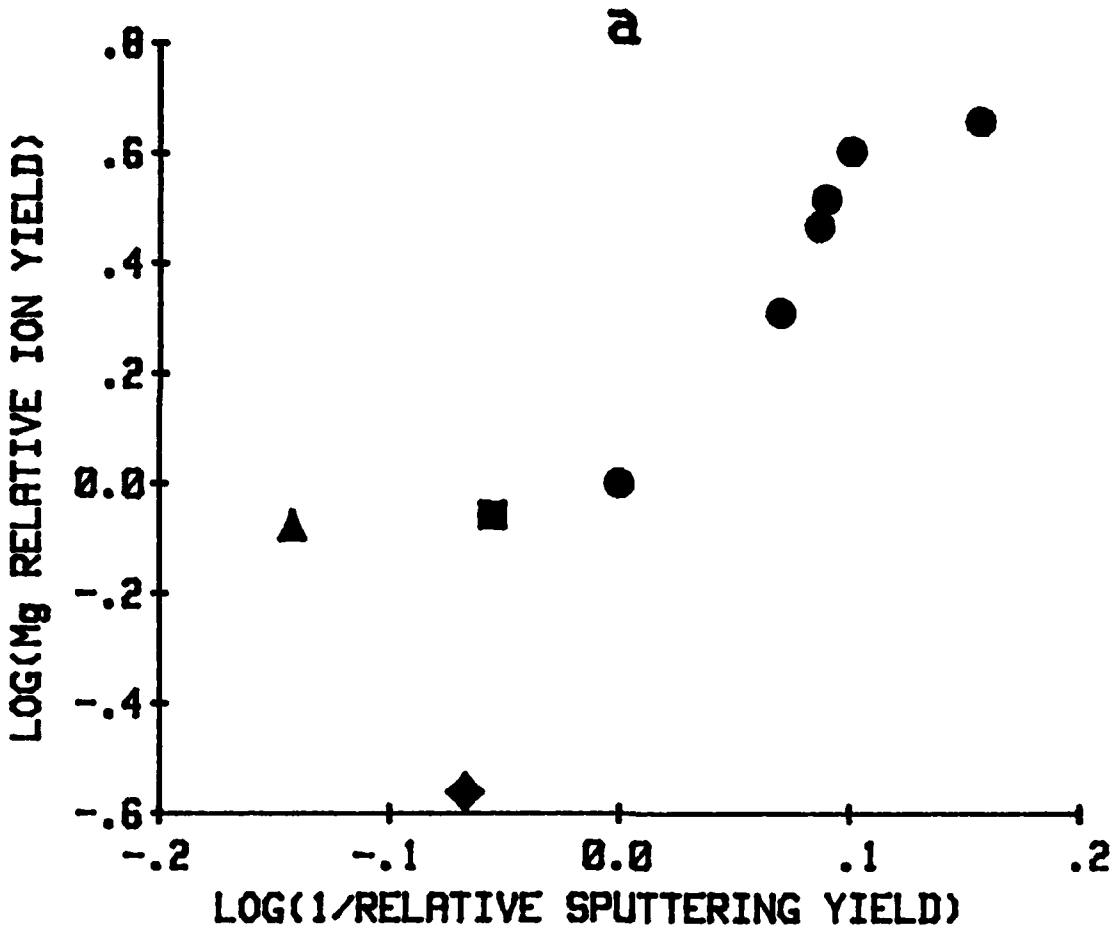
a
.8
.6
.4
.2
0.0
-.2
-.4
-.6
LOG(Mg RELATIVE ION YIELD)
-.2
-.1
0.0
.1
.2
LOG(1/RELATIVE SPUTTERING YIELD)

Fig 4a

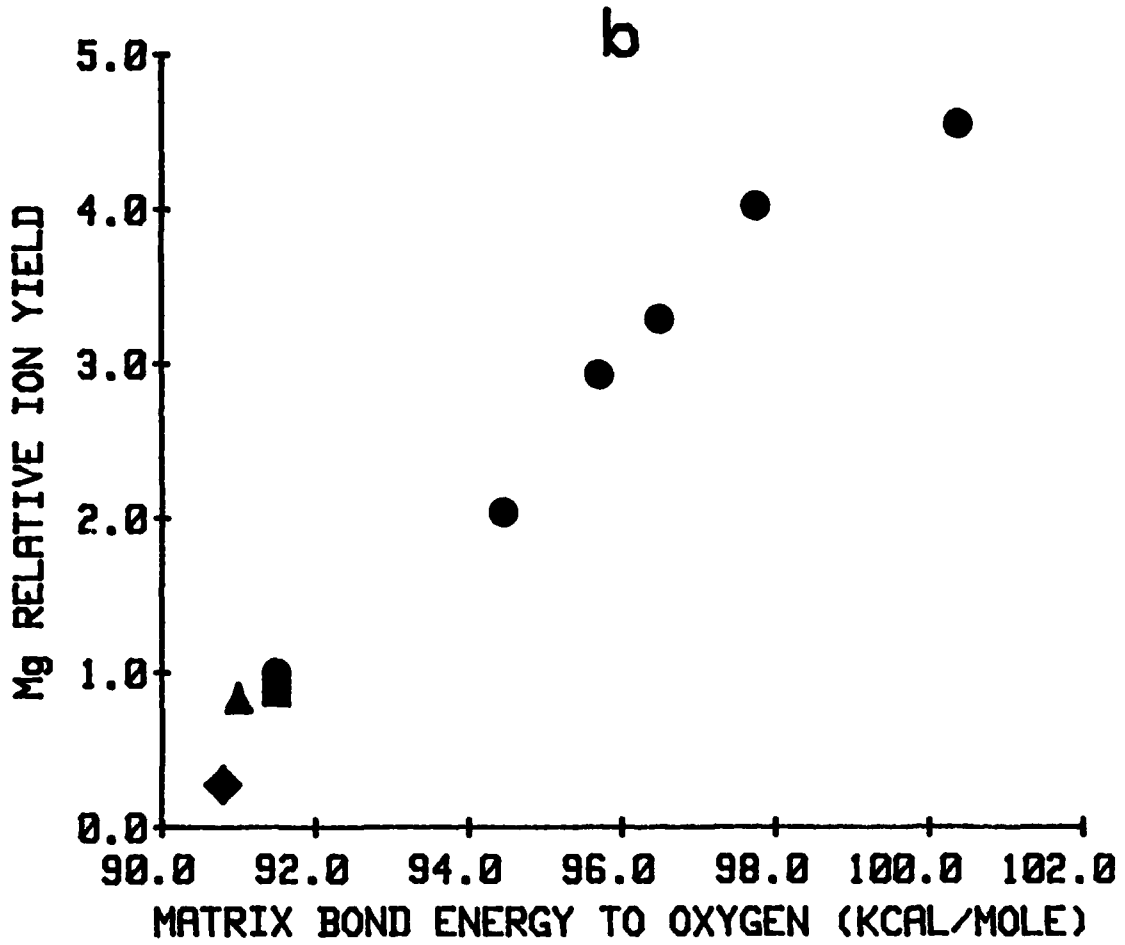
b
5.0
4.0
3.0
2.0
1.0
0.0
Mg RELATIVE ION YIELD
90.0
92.0
94.0
96.0
98.0
100.0
102.0
MATRIX BOND ENERGY TO OXYGEN (KCAL/MOLE)

Fig 4b

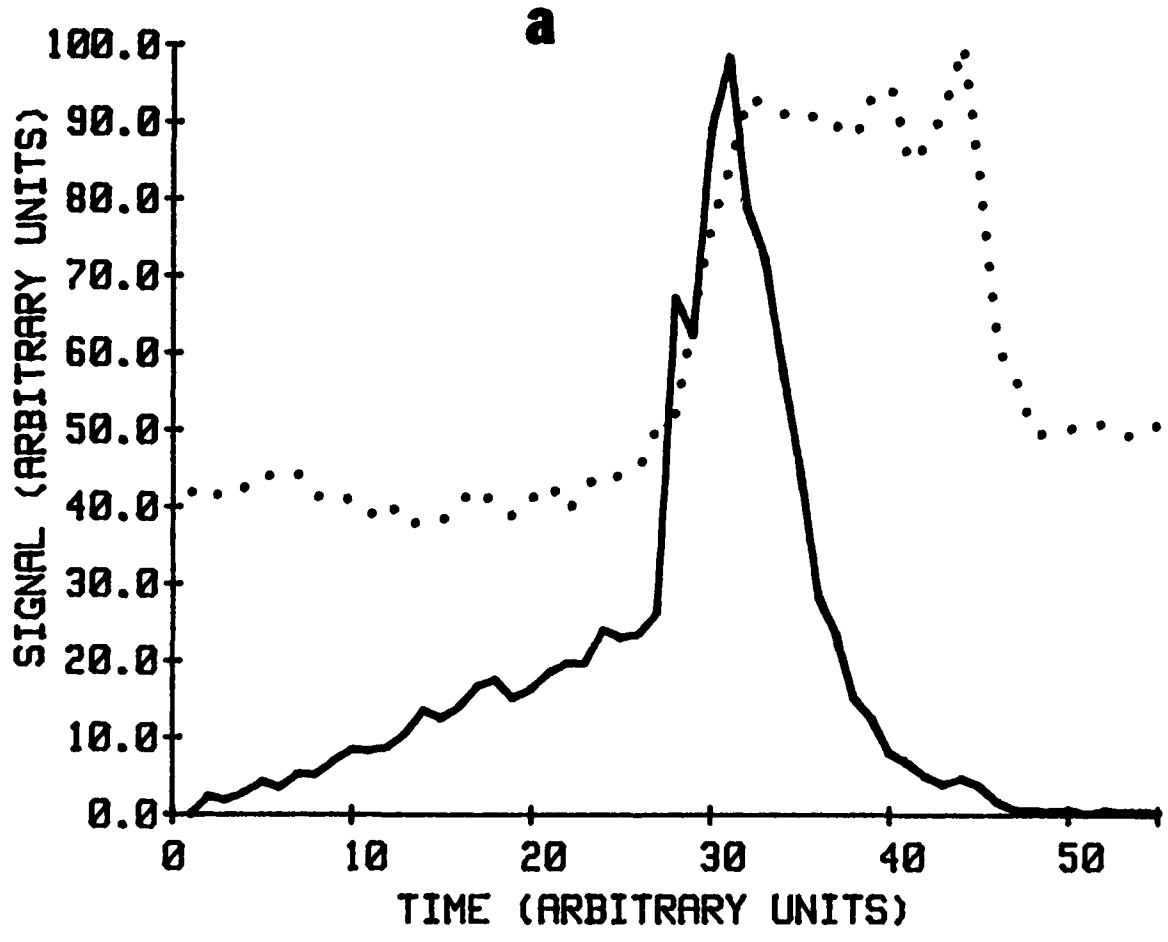
a
100.0
90.0
80.0
70.0
60.0
50.0
40.0
30.0
20.0
10.0
0.0
SIGNAL (ARBITRARY UNITS)
0
10
20
30
40
50
TIME (ARBITRARY UNITS)

Fig 5a

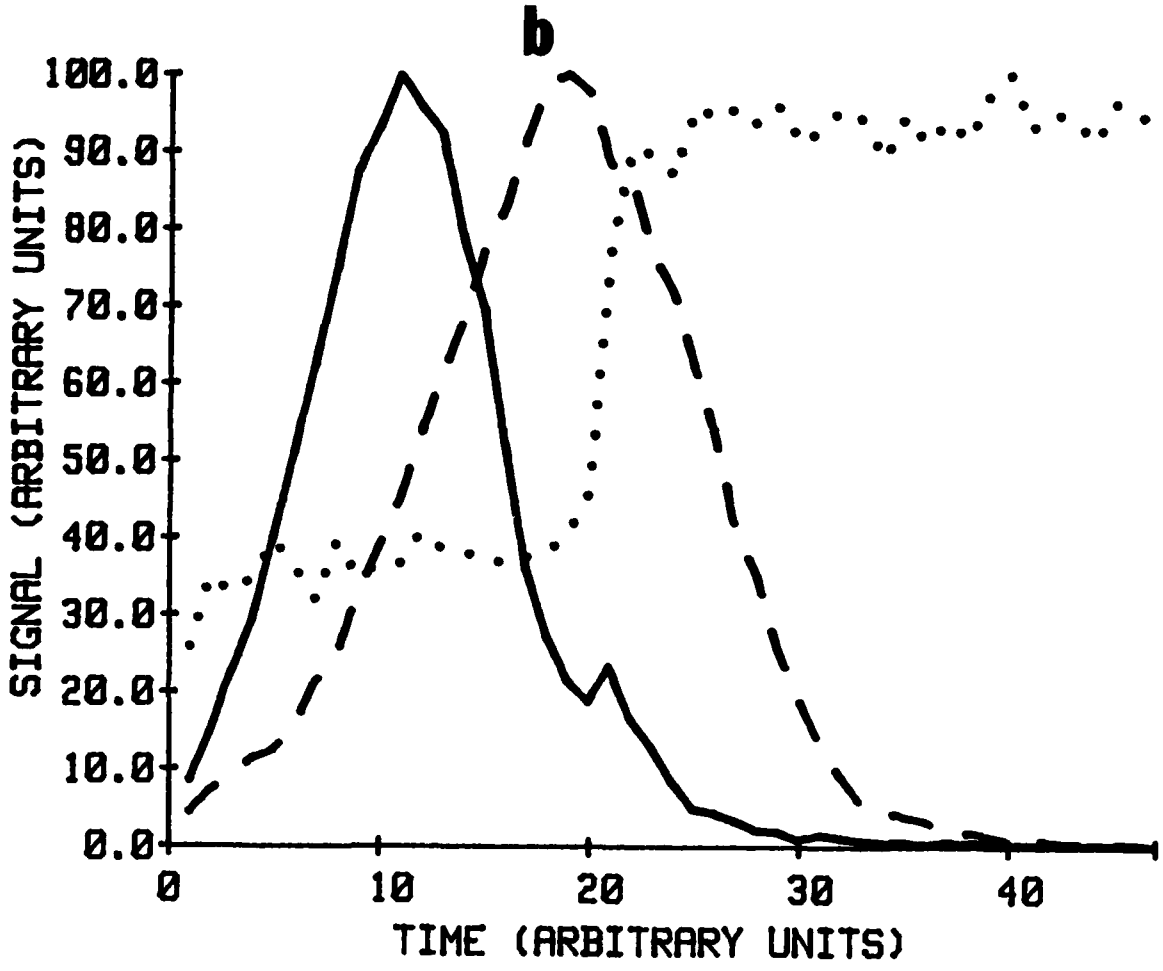
b
100.0
90.0
80.0
70.0
60.0
50.0
40.0
30.0
20.0
10.0
0.0
SIGNAL (ARBITRARY UNITS)
0
10
20
30
40
TIME (ARBITRARY UNITS)

Fig 5b

Fig 6a

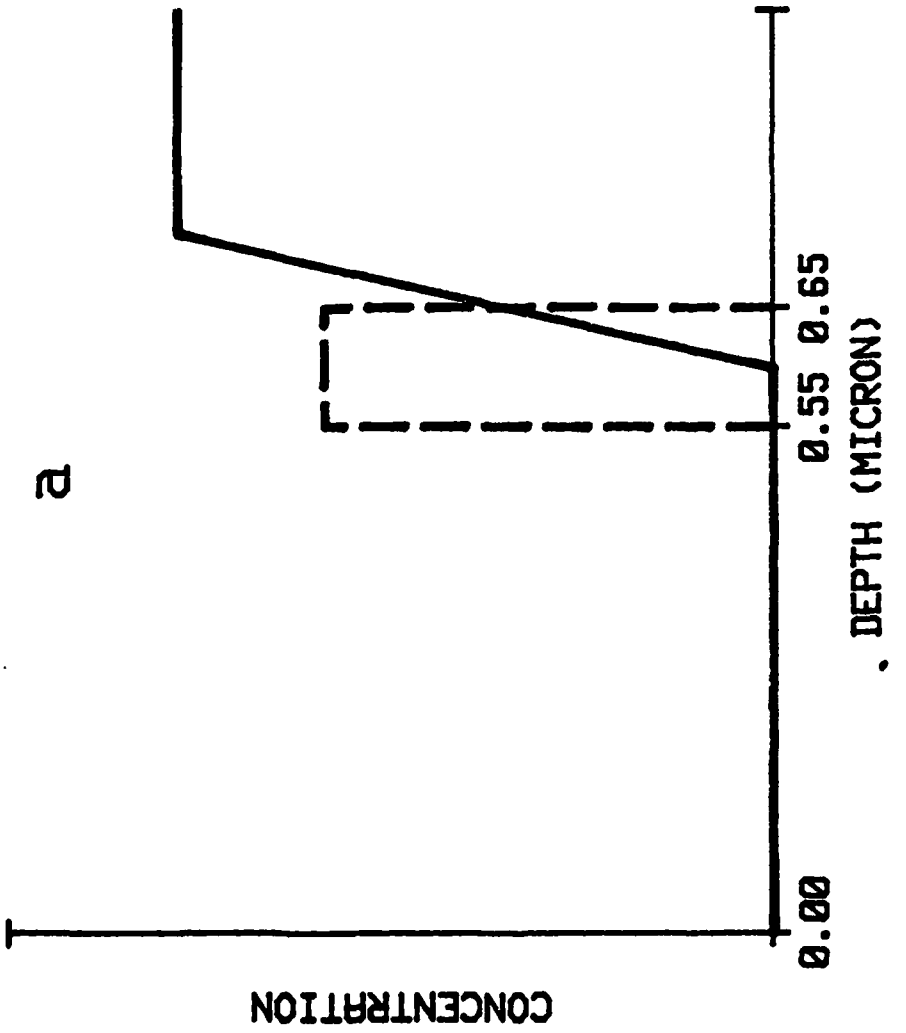

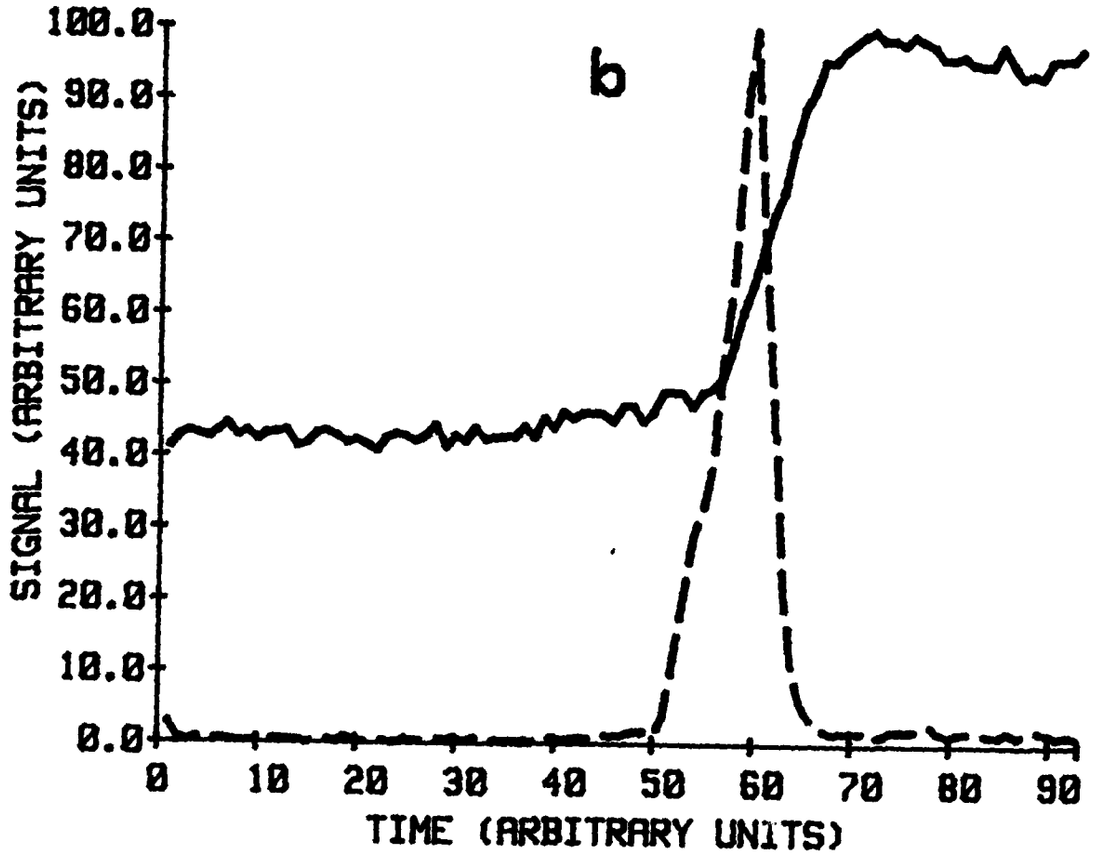
b
SIGNAL (ARBITRARY UNITS)
100.0
90.0
80.0
70.0
60.0
50.0
40.0
30.0
20.0
10.0
0.0
0
10
20
30
40
50
60
70
80
90
TIME (ARBITRARY UNITS)

Fig. 1b

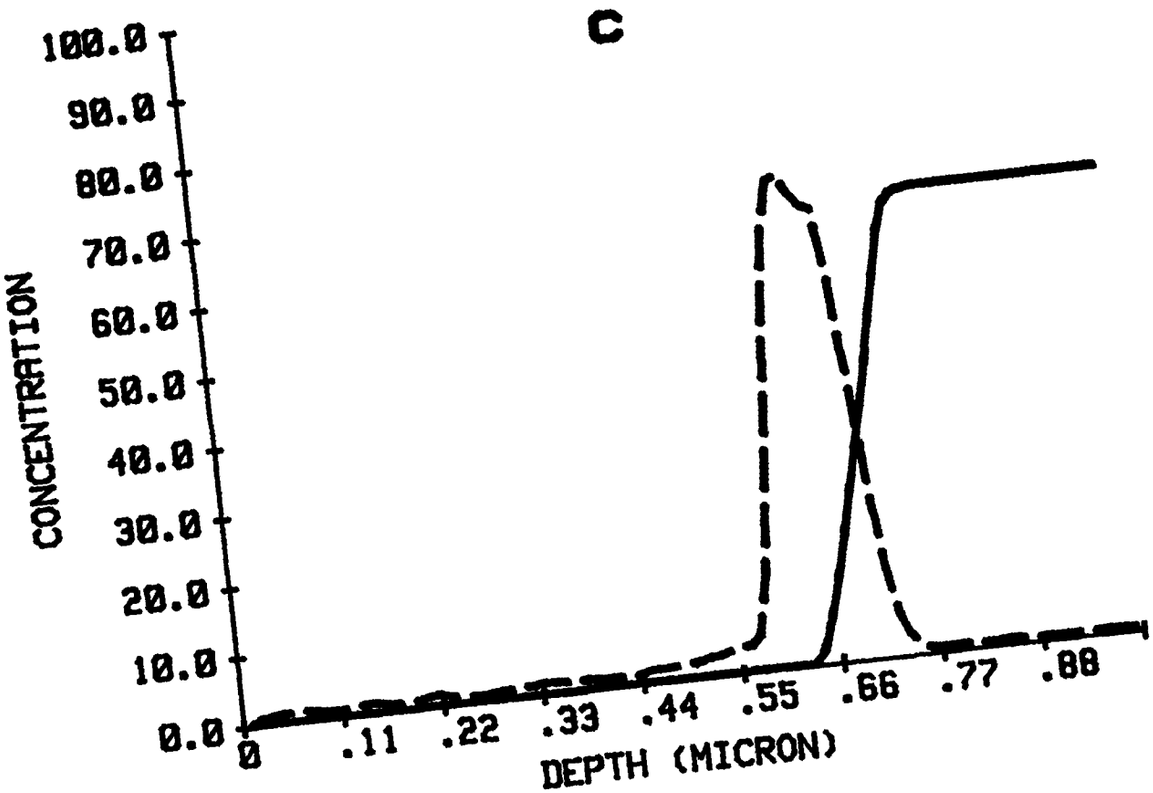
C
100.0
90.0
80.0
70.0
60.0
50.0
40.0
30.0
20.0
10.0
0.0
CONCENTRATION
0
.11
.22
.33
.44
.55
.66
.77
.88
DEPTH (MICRON)

Fig 6c

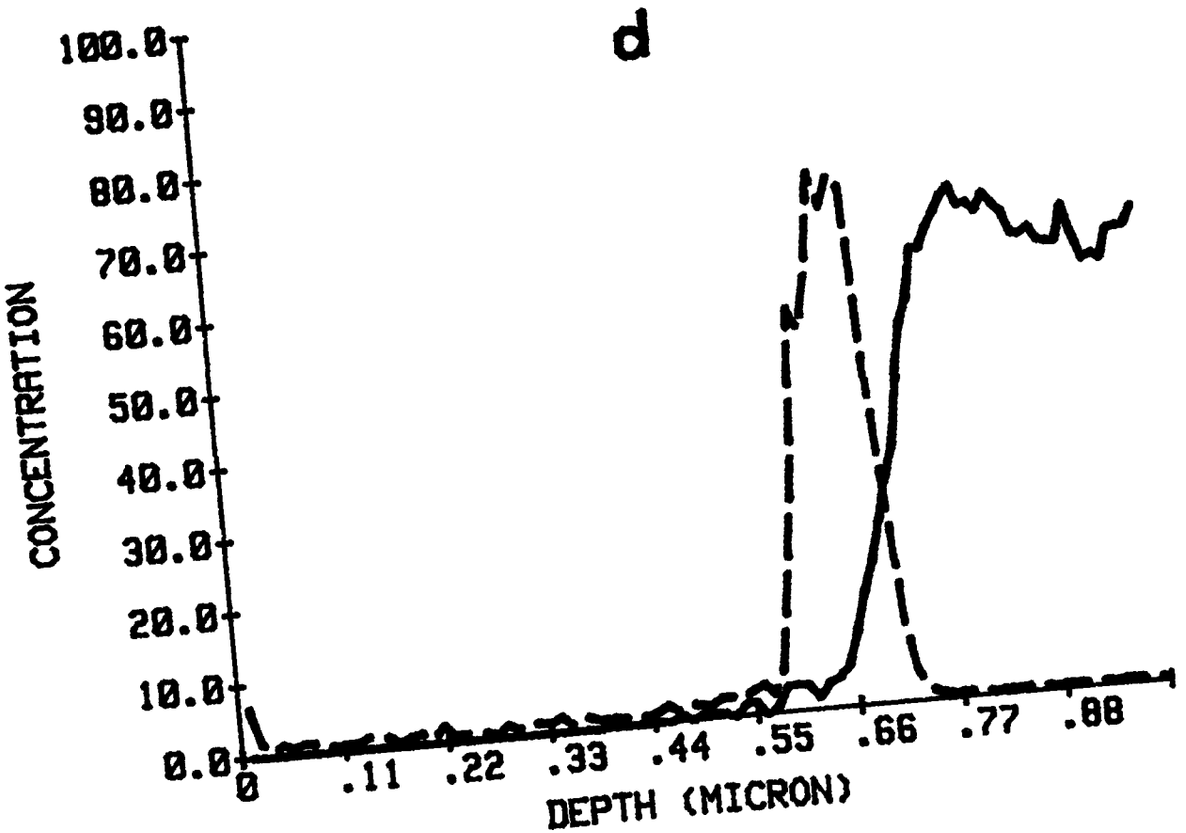
d
100.0
90.0
80.0
70.0
60.0
50.0
40.0
30.0
20.0
10.0
0.0
CONCENTRATION
0
.11
.22
.33
.44
.55
.66
.77
.88
DEPTH (MICRON)

Figure 6J